

The QCD phase diagram at nonzero quark density

G. Endrődi*, Z. Fodor*[†], S.D. Katz*[†], K.K. Szabó[†]

ABSTRACT: We determine the phase diagram of QCD on the $\mu - T$ plane for small to moderate chemical potentials. Two transition lines are defined with two quantities, the chiral condensate and the strange quark number susceptibility. The calculations are carried out on $N_t = 6, 8$ and 10 lattices generated with a Symanzik improved gauge and stout-link improved 2+1 flavor staggered fermion action using physical quark masses. After carrying out the continuum extrapolation we find that both quantities result in a similar curvature of the transition line. Furthermore, our results indicate that in leading order the width of the transition region remains essentially the same as the chemical potential is increased.

KEYWORDS: Lattice QCD Thermodynamics, Sign problem.

*Institute for Theoretical Physics, Eötvös University, H-1117 Budapest, Hungary.

[†]Department of Physics, University of Wuppertal, D-42097 Wuppertal, Germany

Contents

1. Introduction	1
2. Definition of the curvature	2
3. Determination of the Taylor-coefficients	4
4. The μ-dependence of the observables	5
4.1 The strange quark number susceptibility	5
4.2 The chiral condensate	5
5. Simulation setup	7
6. Results	7
7. Acknowledgment	10

1. Introduction

The understanding of the phase diagram of QCD is of utmost importance and has attracted much attention, both experimental and theoretical. Experimental results are coming from cosmology and heavy ion collisions. Recently, in a collision of gold nuclei at the Relativistic Heavy Ion Collider (RHIC), a temperature beyond 200 MeV was reached [1], which indicates that the quark-gluon plasma has been created. Furthermore, the density of the system can be varied by tuning the center of mass energy $\sqrt{s_{NN}}$. While most of the ongoing experiments like those at LHC or RHIC concentrate on achieving very high energies and thus small chemical potentials, there are projects that aim for regions of the phase diagram with larger densities (RHIC II, Facility for Antiproton and Ion Research (FAIR)). In these latter experiments an important objective is to identify the critical endpoint, e.g., by searching for critical opalescence. Designing these next generation experiments can benefit greatly from developing theoretical understanding of the phase diagram.

Our theoretical knowledge about the phase diagram of QCD is mostly limited to the zero chemical potential ($\mu = 0$) axis and obtained by the use of lattice QCD. The main reason that full results for $\mu > 0$ are not available is the infamous sign problem which spoils any lattice technique based on importance sampling. There are various scenarios for the $\mu > 0$ region of the phase diagram, among which two are illustrated in Figure 1.

The transition at $\mu = 0$ is a crossover [2] and we expect that the transition temperature decreases as we increase μ . Besides the actual value of the curvature of the transition line a particularly interesting question is whether the transition becomes weaker or stronger as μ grows. A strengthening of the transition could lead to the existence of a critical point, where the crossover transforms into a true phase transition (see left side of Figure 1). Another possibility is that the transition weakens with increasing μ (see right side of Figure 1). The

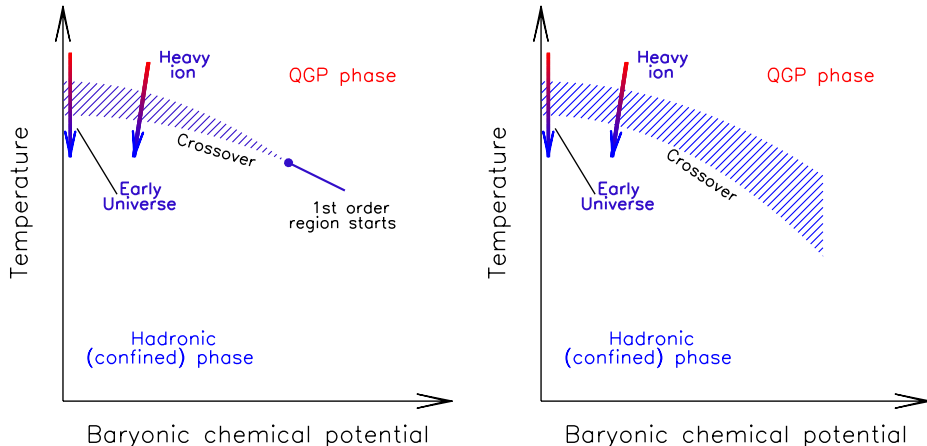


Figure 1: Two possible scenarios for the QCD phase diagram on the $\mu - T$ plane, defined using a given observable. The left panel shows a phase diagram with a transition growing stronger and possibly even turning into a real, first-order phase transition at a critical endpoint. The right panel on the other hand corresponds to a scenario with a weakening transition and no critical endpoint. The paths corresponding to systems describing the early Universe and a heavy ion collision are also shown by the arrows. Note that different observables may lead to different scenarios.

existence of the critical point would not be ruled out by such a scenario but would require non-monotonic behavior [3].

At zero chemical potential lattice calculations provide reliable and accurate results [4–9]. Much more difficult is the situation at nonzero chemical potential. Simulations at non-vanishing chemical potential are burdened by the sign (complex action) problem: the fermion determinant here becomes complex, and as a result makes Monte-Carlo methods based on importance sampling impossible. Recently several methods were developed to access the region of small chemical potentials. They are all based on simulations at zero or purely imaginary chemical potentials where the sign problem is absent. The first possibility is the reweighting of the generated configurations [10–14]. The weight factors can also be approximated by a Taylor expansion in μ [15–19]. Further possibilities are an analytic continuation from imaginary μ [20–27], or using the canonical ensemble [28–30]. The above studies were carried out on coarse lattices and in most cases with non-physical quark masses. We emphasize that to have a full result, the use of physical quark masses and a reliable continuum extrapolation are essential. In this paper we determine the transition temperature $T_c(\mu)$ as a function of the chemical potential through a Taylor-expansion technique. The first term of this expansion is zero due to the symmetry $\mathcal{Z}(\mu) = \mathcal{Z}(-\mu)$ of the partition function. Therefore the first nonvanishing contribution comes from the second order, which is related to the curvature of the transition line.

2. Definition of the curvature

Let us parameterize the transition line in the vicinity of the vertical $\mu = 0$ axis as

$$T_c(\mu^2) = T_c (1 - \kappa \cdot \mu^2 / T_c^2) \quad (2.1)$$

with T_c being short for $T_c(0)$. This implies that the curvature can be written as

$$\kappa = -T_c \left. \frac{dT_c(\mu^2)}{d(\mu^2)} \right|_{\mu=0} \quad (2.2)$$

where (and also in the following) μ refers to the baryonic chemical potential ($\mu \equiv \mu_B = 3\mu_{u,d}$), where $\mu_{u,d}$ is the quark chemical potential assigned to the light quarks. Thus one has to measure T_c as a function of μ for small chemical potentials. To this end we use a definition of T_c which is most suitable for determining the curvature.

Let us consider a quantity $\phi(T, \mu^2)$ that is monotonic in T in the transition region, and fulfills the following constraints:

$$\lim_{T \rightarrow 0} \frac{\partial}{\partial \mu^2} \phi(T, \mu^2) = 0, \quad \lim_{T \rightarrow \infty} \frac{\partial}{\partial \mu^2} \phi(T, \mu^2) = 0 \quad (2.3)$$

that is to say, ϕ does not depend on the chemical potential in the limiting cases $T \rightarrow 0$ and $T \rightarrow \infty$. For any fixed μ we can define a transition temperature $T_c(\mu^2)$ as the temperature at which $\phi(T, \mu^2)$ takes the predefined constant value C :

$$\phi(T, \mu^2) \Big|_{T=T_c(\mu^2)} = C. \quad (2.4)$$

We will choose a C that corresponds to the inflection point of $\phi(T, 0)$. (Note that T_c can also be defined as the location of the maximum or inflection point of some observable. At non-zero μ this turns out to be somewhat less advantageous since a fitting of the reweighted data is required.)

Now let us determine the curvature using this definition of $T_c(\mu^2)$. The total derivative of the observable $\phi(T, \mu^2)$ may be written as

$$d\phi = (\partial\phi/\partial T) \Big|_{\mu=0} \cdot dT + (\partial\phi/\partial(\mu^2)) \Big|_{\mu=0} \cdot d\mu^2 \quad (2.5)$$

Along the $T_c(\mu^2)$ line, ϕ is constant by definition, thus $d\phi = 0$. One obtains

$$\frac{dT_c}{d\mu^2} = - \underbrace{\left(\frac{\partial\phi}{\partial\mu^2} \right) \Big|_{T=T_c, \mu=0} / \left(\frac{\partial\phi}{\partial T} \right) \Big|_{T=T_c, \mu=0}}_{R(T)} \quad (2.6)$$

Thus, for every C we can define a curvature. Since the $T_c(C)$ function is invertible for the whole C range, we can also write (2.6) as a function of temperature, $R(T)$.

The function $R(T)$ is related to the distance that the $\phi(T)$ curve shifts along the T axis as the chemical potential is varied. Given $\phi(T)$ and $R(T)$ at zero chemical potential, the shift for non-zero μ at leading order is $R(T) \cdot \mu^2$ (the curve moves to the left if $R(T)$ is negative and to the right otherwise). This behavior is illustrated in Figure 2. Using $R(T)$ we can define a temperature dependent curvature according to (2.2) as $\kappa(T) = -T_c \cdot R(T)$. The meaning of $\kappa(T)$ is again simple: it gives the curvature of the $\phi = \text{const.}$ curve which starts from T at $\mu = 0$.

We use the value of $\kappa(T)$ at $T = T_c$ to define the curvature for a given observable. The shape of the $\kappa(T)$ function also has important consequences. The slope of $\kappa(T)$ around T_c is related to the width of the transition as follows: if the slope is zero, i.e. $\kappa(T)$ is

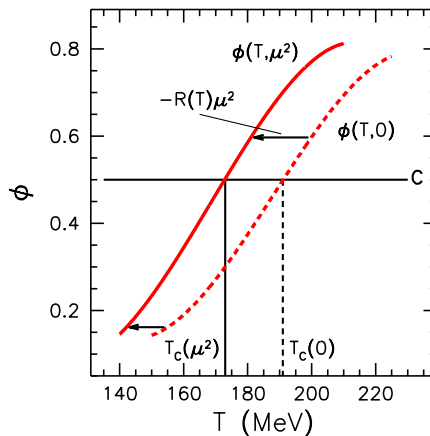


Figure 2: Illustration of the behavior of the observable ϕ at $\mu = 0$ and $\mu > 0$. The quantity $T_c(\mu^2)$ is defined as the temperature where $\phi(T, \mu^2)$ crosses a constant value C . For $\mu > 0$, each point of the $\phi(T, 0)$ curve shifts in T by $R(T) \cdot \mu^2$ (see definition in text).

constant around T_c , then all points shift the same amount along the T axis when a small chemical potential is switched on. This means that to leading order in μ the shape of the $\phi(T)$ function (and thus, the width of the transition) does not change. If the slope is positive, then points with larger T shift more than the ones with smaller T resulting in a compression of points, i.e. a narrower transition. Similarly, a negative slope indicates a broadening of the transition.

All in all, the expression $\partial\kappa/\partial T$ is therefore related to the relative change in the width $W(\mu)$ of the transition as the chemical potential increases:

$$\frac{1}{W} \frac{\partial W}{\partial(\mu^2)} = - \frac{1}{T_c} \frac{\partial T_c}{\partial T} \Big|_{T=T_c}$$

where we assume that W is proportional to the inverse slope of the quantity in question: $W \sim |(\partial\phi/\partial T|_{T=T_c})^{-1}|$.

The two observables we use are the renormalized chiral condensate $\phi = \langle \bar{\psi}\psi_r \rangle$ and the normalized strange quark number susceptibility $\phi = \langle \chi_s/T^2 \rangle$. As we show in section 4, both satisfy the constraints listed in (2.3). The derivative $\partial\phi/\partial T$ is determined numerically, using the $\mu = 0$ data as a function of the temperature. In order to calculate the derivative $\partial\phi/\partial(\mu^2)$ we need to measure more complicated operators; the technique for computing these is detailed in the next section.

3. Determination of the Taylor-coefficients

Let us consider the partition function of the staggered lattice formulation for N_f fermion flavors in its usual form

$$\mathcal{Z} = \int \mathcal{D}U e^{-S_g(U)} (\det M)^{N_f/4} \quad (3.1)$$

and denote the derivative with respect to $\mu_{u,d}$ by $'$. The derivatives of \mathcal{Z} are easily calculated to be $(\log \mathcal{Z})' = \langle n_{u,d} \rangle$ and $(\log \mathcal{Z})'' = \langle n_{u,d}^2 + n'_{u,d} \rangle - \langle n_{u,d} \rangle^2$, where the light quark number

density $n_{u,d}$ and its derivative with respect to $\mu_{u,d}$ are given by the following combinations:

$$n_{u,d} = \frac{N_f}{4} \text{Tr} (M^{-1} M')$$

$$n'_{u,d} = \frac{N_f}{4} \text{Tr} (M^{-1} M'' - M^{-1} M' M^{-1} M')$$

Using these definitions the second derivative of any (possibly explicitly μ -dependent) observable can be straightforwardly determined. For the renormalized chiral condensate and the strange quark number susceptibility (see definition in section 4) one obtains:

$$\left. \frac{\partial^2 \langle \bar{\psi} \psi_r \rangle}{\partial \mu_{u,d}^2} \right|_{\mu_{u,d}=0} = \langle \bar{\psi} \psi_r (n_{u,d}^2 + n'_{u,d}) \rangle - \langle \bar{\psi} \psi_r \rangle \langle n_{u,d}^2 + n'_{u,d} \rangle + \langle 2\bar{\psi} \psi'_r n_{u,d} + \bar{\psi} \psi''_r \rangle \quad (3.2)$$

$$\left. \frac{\partial^2 \langle \chi_s \rangle}{\partial \mu_{u,d}^2} \right|_{\mu_{u,d}=0} = \langle \chi_s (n_{u,d}^2 + n'_{u,d}) \rangle - \langle \chi_s \rangle \langle n_{u,d}^2 + n'_{u,d} \rangle - 2 \langle n_s n_{u,d} \rangle^2 \quad (3.3)$$

where n_s is the strange quark number density, defined similarly as $n_{u,d}$. Note that the additive renormalization of $\bar{\psi} \psi_r$ (see section 4.2) does not influence the derivative in question.

For the chiral condensate – being a μ -dependent operator – the derivatives $\bar{\psi} \psi'_r$ and $\bar{\psi} \psi''_r$ of this explicit dependence are also present in (3.2). These terms were calculated numerically, using a purely imaginary chemical potential $\Delta\mu_i$. The value of $\Delta\mu_i$ was varied in the range $0.01 \dots 0.0005$, and it was checked that the finite differences converge fast enough to the $\Delta\mu_i \rightarrow 0$ values and the error coming from this approximation is negligible compared to statistical errors. Taking into account these considerations $\Delta\mu_i = 0.001$ was used.

4. The μ -dependence of the observables

We calculated the curvature of the transition line using the strange quark number susceptibility and the chiral condensate. The details of their renormalization and behavior are explained in this section.

4.1 The strange quark number susceptibility

The strange quark number susceptibility is defined as

$$\langle \chi_s \rangle = \frac{T}{V} \frac{\partial^2 \log \mathcal{Z}}{\partial \mu_s^2} \quad (4.1)$$

This observable needs no renormalization, since it is connected to a conserved current. It is useful to study the combination $\langle \chi_s / T^2 \rangle$, since it obeys the conditions of (2.3). It is easy to see that at $T = 0$ one gets $\langle \chi_s / T^2 \rangle = 0$ and at $T \rightarrow \infty$ the normalized quark number susceptibility $\langle \chi_s / T^2 \rangle$ reaches its $\mu_{u,d}$ independent Stefan-Boltzmann limit of 1.

4.2 The chiral condensate

The chiral condensate can also be expressed as a derivative of the partition function:

$$\langle \bar{\psi} \psi \rangle = \frac{T}{V} \frac{\partial \log \mathcal{Z}}{\partial m} \quad (4.2)$$

The renormalization of $\bar{\psi}\psi$ is a more delicate issue as compared to the situation with χ_s . The free energy ($\log \mathcal{Z}$) contains additive divergences in the cutoff. In order to carry out the proper renormalization of the condensate, these additive divergences have to be eliminated – this is done by subtracting the $T = 0$ contribution.

The multiplicative divergence due to the derivative with respect to the mass can be eliminated with a multiplication by the bare quark mass. Then, in order to have a dimensionless combination¹, the whole expression can be divided by the fourth power of some dimensionful mass scale, Q^4 :

$$\langle \bar{\psi}\psi_r \rangle = (\langle \bar{\psi}\psi \rangle - \langle \bar{\psi}\psi \rangle(T=0)) \cdot m \cdot \frac{1}{Q^4} \quad (4.3)$$

This way no divergent contributions remain: this is a meaningful quantity to study in the continuum limit.² In this work we use the $T = 0$ pion mass for the Q normalization scale.

The final condition that has to be satisfied is that $\langle \bar{\psi}\psi_r \rangle$ should be independent of μ at $T = 0$ and $T \rightarrow \infty$. At $T = 0$ the partition function is independent of μ as long as μ is smaller than a μ_c critical value (the approximate baryon mass) and no baryons can be created from the vacuum. Only for $\mu > \mu_c$ does the partition function have a non-trivial μ dependence. Therefore all derivatives of \mathcal{Z} (thus $\langle \bar{\psi}\psi_r \rangle$) are independent of μ for $\mu < \mu_c$. The chemical potential regime covered in this paper lies in this region. In the Stefan-Boltzmann limit ($T \rightarrow \infty$) the μ independence is only satisfied in the sense $(\bar{\psi}\psi_r)^{-1} \partial/\partial\mu^2(\bar{\psi}\psi_r) \rightarrow 0$. Figure 4 demonstrates, however, that for temperatures above the transition region $\bar{\psi}\psi_r$ is already practically independent of μ .

Figure 3 illustrates the behavior of $\langle \chi_s/T^2 \rangle$ and $\langle \bar{\psi}\psi_r \rangle$ as a function of the temperature, determined on $N_t = 10$ lattices.

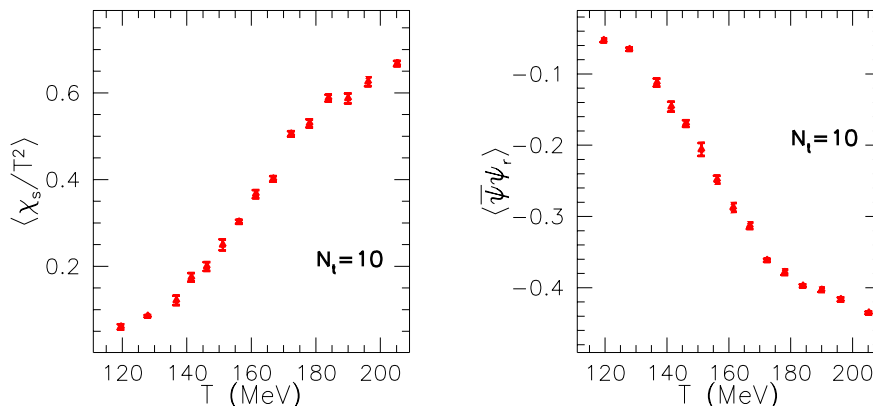


Figure 3: The strange susceptibility and the renormalized chiral condensate as functions of the temperature at $\mu = 0$.

¹Note that a division by T^4 which would also render the condensate dimensionless, changes the temperature dependence and would lead to a non-monotonic T dependence, which would be disadvantageous in the present context.

²Note that this renormalization procedure leads to a somewhat unusual chiral condensate which vanishes at $T = 0$ and reaches a negative value at $T \rightarrow \infty$. A more conventional condensate which is positive at $T = 0$ and goes to zero at large temperatures can be obtained by a constant shift which is irrelevant for our present study.

5. Simulation setup

We used a Symanzik improved gauge and stout-link improved staggered fermionic lattice action in order to reduce taste violation [5]. The configurations were generated with an exact RHMC algorithm [31]. We determined the line of constant physics (LCP) using physical masses for the light quarks $m_{u,d}$ as well as for the strange quark m_s . The LCP was fixed by setting the ratios m_K/f_K and m_K/m_π to their physical values. We used three different lattice spacings $N_t = 6, 8, 10$ and aspect ratios N_s/N_t of 4 and 3. The scale was fixed by f_K and its unambiguity was checked by calculating m_{K^*} , f_π and r_0 . The random noise estimator method was used to measure the operators detailed in section 3. We used 80 random vectors so that the error coming from the method and the statistical error are of the same extent. The details of the simulation setup can be found elsewhere [5, 32]. We used the gauge ensembles generated for a $\mu = 0$ study [5]. We also generated extra configurations for $N_t = 8$ and 10. The number of trajectories at each β , N_s and N_t is summarized in table 1. The autocorrelation times were below 10 trajectories in all cases. After confirming the absence of thermalization effects, we measured observables on every fifth trajectory. The measurements were performed on clusters equipped with graphics cards [33].

$N_s^3 \times N_t$	β	#of trajecs.	$N_s^3 \times N_t$	β	#of trajecs.	$N_s^3 \times N_t$	β	#of trajecs.
$24^3 \times 6$	3.4500	1750	$24^3 \times 8$	3.6000	1800	$28^3 \times 10$	3.6500	800
	3.4950	2500		3.6250	2100		3.6750	3350
	3.5100	5200		3.6375	4050		3.7000	800
	3.5250	5350		3.6500	5000		3.7125	850
	3.5400	5450		3.6625	3150		3.7250	800
	3.5550	3400		3.6750	3200		3.7375	800
	3.5700	3350		3.6813	3200		3.7500	2300
	3.5850	4650		3.6875	14350		3.7625	800
	3.6000	3000		3.7000	2100		3.7750	5950
	3.6450	3650		3.7160	3050		3.7875	4200
$18^3 \times 6$	3.5550	4550	3.7400	2850	3.8000		1600	
					3.8125		2000	
					3.8250		4850	
					3.8375		4150	
					3.8550		5950	

Table 1: Number of trajectories for various lattice geometries.

6. Results

First we checked finite size effects by comparing our results at $\beta = 3.555$ obtained on $24^3 \times 6$ and on $18^3 \times 6$ lattices. This value of β corresponds to about 155 MeV, i.e. is near the pseudocritical temperature. The larger box is of physical size ~ 5 fm. We observe a good agreement as the results for $\partial\phi/\partial(\mu^2)$ agree within statistical errors for both the chiral condensate $\phi = \langle \bar{\psi}\psi_r \rangle$ and the strange quark number susceptibility $\phi = \langle \chi_s/T^2 \rangle$. Figure 4 shows our $N_t = 6$ results for $N_s = 24$ and $N_s = 18$. Thus we conclude that finite size errors can be neglected at the present statistical accuracy.

Since the actual shape of the $\kappa(T)$ function is unknown we carry out a Taylor expansion around T_c in the $t = (T - T_c)/T_c$ dimensionless variable:

$$\kappa(T) = \kappa(T_c) + c_0 \cdot t + c_1 \cdot t^2 \quad (6.1)$$

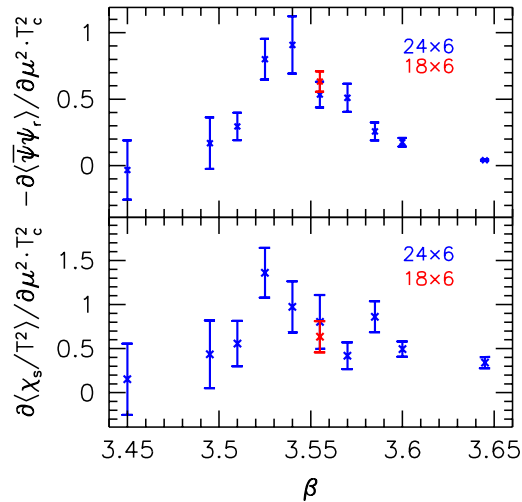


Figure 4: The derivative of our observables with respect to μ^2 measured on $N_t = 6$ lattices. The $N_s = 24$ results (blue points) are checked at one temperature by $N_s = 18$ (red point). In the case of both observables a good agreement is observed, which indicates that finite size effects are small as compared to statistical errors.

For each lattice spacing (i.e. each N_t) we have several simulation points, corresponding to different temperatures. In order to fit all of our points at once, we allow a lattice spacing dependence for the constant and linear terms (having a lattice spacing dependence of the quadratic term is also possible, but it does not improve the quality of the fits). Therefore we fit all of our simulation points with the following function

$$\kappa(T; N_t) = \kappa(T_c; \text{cont}) + c_0 \cdot t + c_1 \cdot t^2 + c_2/N_t^2 + c_3 \cdot t/N_t^2 \quad (6.2)$$

with fit parameters $\kappa(T_c; \text{cont})$, c_0 , c_1 , c_2 and c_3 . The independent data points as well as the fitted curves (for each N_t and in the continuum) are shown in Figure 5.

The $\chi^2/\text{d.o.f.}$ values of the two fits are 1.19 and 1.29, respectively, indicating good fit qualities. The continuum curvatures are given by the $\kappa(T_c; \text{cont})$ fit parameter, while the relative change in the width of the transition can be read off from $-c_0$. Our final results are

$$\begin{aligned} \kappa(\chi_s/T^2) &= 0.0089(14), & \kappa(\bar{\psi}\psi_r) &= 0.0066(20) \\ \Delta W/W(\chi_s/T^2) &= 0.033(16), & \Delta W/W(\bar{\psi}\psi_r) &= 0.030(18) \end{aligned}$$

The results obtained from the two quantities are consistent with each other. Using the κ values we can give the transition lines defined by any of the observables as

$$T_c(\mu) = T_{c;\mu=0} [1 - \kappa \cdot \mu^2 / T_{c;\mu=0}^2] \quad (6.3)$$

The results for $\Delta W/W$ also suggest that the transition remains a weak crossover with essentially constant strength for small to moderate chemical potentials. Actually, there is a slight increase in the width of the transition determined from both quantities. This effect is, however, very weak: the width only changes by a few percent up to $\mu \approx T_c$. This

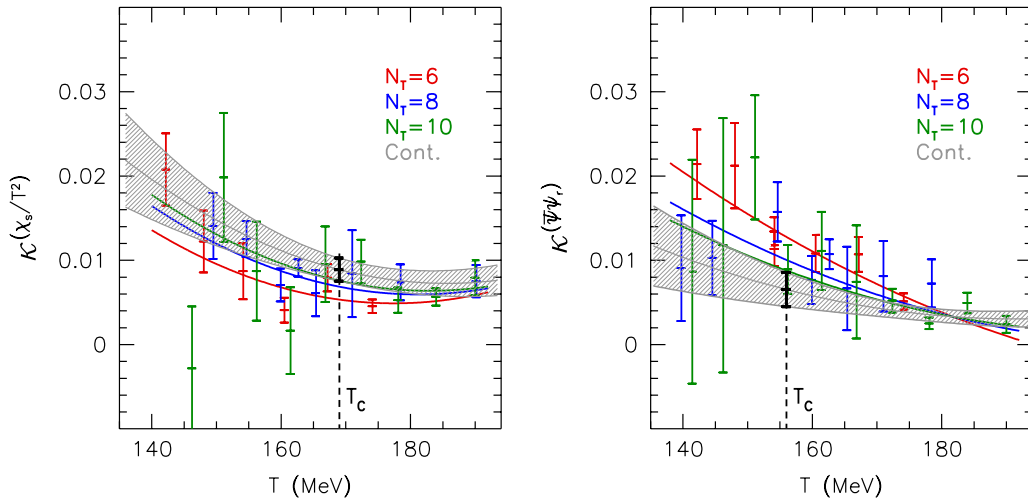


Figure 5: The curvature $\kappa(T)$ (see definition in text) determined using the strange quark number susceptibility (left) and the renormalized chiral condensate (right), respectively. A result of the combined fit (described in the text) is shown by the gray band. The fit results for the individual $N_t = 6, 8, 10$ lattices are shown by the red, blue and green curves. The width of the gray band corresponds to the statistical uncertainty of the fit.

finding is consistent with previous results in the literature. In Ref. [13] the imaginary parts of the Lee-Yang zeroes of the partition function were studied with exact reweighting. At sufficiently high μ the Lee-Yang zeroes approached the real axis, thus leading to a critical point. However, around $\mu = 0$ an opposite effect can be observed, the Lee-Yang zeroes slightly move away from the real axis, indicating a weakening of the transition. In Refs [25] (3 flavors) and [27] (2+1 flavors) the critical surface in the quark masses – chemical potential space was studied and the curvature of the surface suggests a weakening of the transition as the chemical potential is increased. Since all these leading order results predict a weakening of the transition for real chemical potentials (i.e. $\mu^2 > 0$), a strengthening is expected in the imaginary direction ($\mu^2 < 0$). It is interesting to note that these leading order results are of the same order of magnitude in the sense that using an extreme extrapolation they all lead to a critical point for an imaginary chemical potential $\mu_q = i \cdot \mu_I$ in the range $\mu_I/T \approx 1 - 3$.

The validity range of our result is difficult to estimate from the present study alone. A conservative estimate for the limit where the result obtained through the Taylor-expansion is still reliable is $\mu_{u,d} \approx T_c$ i.e. where the expansion parameter exceeds unity. In the baryonic chemical potential this corresponds to about 500 MeV. Beyond this limit higher-order corrections are by all means expected to be important. Earlier experience with the exact reweighting method [13] also shows that the leading-order quadratic behavior of the $T_c(\mu)$ function dominates upto the above mentioned limit in the baryonic chemical potential. To investigate whether higher order terms may lead to a critical point one must carry out a similar analysis with full reweighting, beyond the reach of present computational resources.

Our final result is shown in Figure 6. The crossover region's extent changes little as the chemical potential increases, and within it two definitions give different curves for $T_c(\mu)$. It is useful to compare the whole picture to the freeze-out curve [34] which summarizes

experimental results on the $\{T, \mu\}$ points where hadronization of the quark-gluon plasma was observed. This curve is expected to lie in the interior of the crossover region, as is indicated by our results as well.

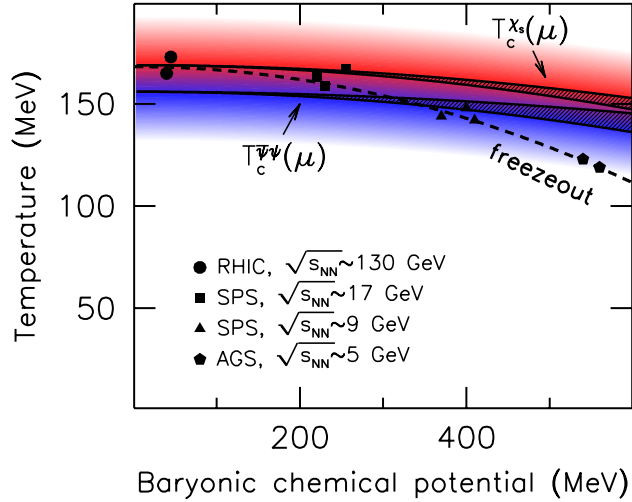


Figure 6: The crossover transition between the ‘cold’ and ‘hot’ phases is represented by the coloured area (blue and red correspond to the transition regions obtained from the chiral condensate and the strange susceptibility, respectively). The lower solid band shows the result for $T_c(\mu)$ defined through the chiral condensate and the upper one through the strange susceptibility. The width of the bands represent the statistical uncertainty of $T_c(\mu)$ for the given μ coming from the error of the curvature κ for both observables. The dashed line is the freeze-out curve from heavy ion experiments [34]. Also indicated are with different symbols the individual measurements of the chemical freeze-out from RHIC, SPS (Super Proton Synchrotron) and AGS (Alternating Gradient Synchrotron), respectively. The center of mass energies $\sqrt{s_{NN}}$ for each are shown in the legend.

7. Acknowledgment

We thank T. Csörgő, C. Schroeder and G.I. Veres for useful discussion. Computations were performed on the BlueGene at FZ Jülich and on clusters at Wuppertal and Budapest. This work is supported in part by DFG grants SFB-TR 55, FO 502/1-2 and the EU grant (FP7/2007-2013)/ERC n°208740.

References

- [1] A. Adare *et al.* [PHENIX Collaboration], Phys. Rev. C **81**, 034911 (2010) [arXiv:0912.0244 [nucl-ex]].
- [2] Y. Aoki, G. Endrődi, Z. Fodor, S. D. Katz and K. K. Szabó, Nature **443**, 675 (2006) [arXiv:hep-lat/0611014].
- [3] J. I. Kapusta and E. S. Bowman, PoS C **POD2009**, 018 (2009) [arXiv:0908.0726 [nucl-th]].
- [4] M. Cheng *et al.*, Phys. Rev. D **74**, 054507 (2006) [arXiv:hep-lat/0608013].
- [5] Y. Aoki, Z. Fodor, S. D. Katz and K. K. Szabó, Phys. Lett. B **643**, 46 (2006) [arXiv:hep-lat/0609068].
- [6] Y. Aoki, S. Borsányi, S. Durr, Z. Fodor, S. D. Katz, S. Krieg and K. K. Szabó, JHEP **0906**, 088 (2009) [arXiv:0903.4155 [hep-lat]].
- [7] A. Bazavov *et al.*, Phys. Rev. D **80**, 014504 (2009) [arXiv:0903.4379 [hep-lat]].
- [8] S. Borsanyi, Z. Fodor, C. Hoelbling, S. D. Katz, S. Krieg, C. Ratti and K. K. Szabo [Wuppertal-Budapest Collaboration], JHEP **1009**, 073 (2010) [arXiv:1005.3508 [hep-lat]].
- [9] S. Borsanyi *et al.*, JHEP **1011**, 077 (2010) [arXiv:1007.2580 [hep-lat]].
- [10] Z. Fodor and S. D. Katz, Phys. Lett. B **534**, 87 (2002) [arXiv:hep-lat/0104001].
- [11] Z. Fodor and S. D. Katz, JHEP **0203**, 014 (2002) [arXiv:hep-lat/0106002].
- [12] F. Csikor, G. I. Egri, Z. Fodor, S. D. Katz, K. K. Szabó and A. I. Tóth, JHEP **0405**, 046 (2004) [arXiv:hep-lat/0401016].
- [13] Z. Fodor and S. D. Katz, JHEP **0404**, 050 (2004) [arXiv:hep-lat/0402006].
- [14] Z. Fodor, S. D. Katz and C. Schmidt, JHEP **0703**, 121 (2007) [arXiv:hep-lat/0701022].
- [15] C. R. Allton *et al.*, Phys. Rev. D **66**, 074507 (2002) [arXiv:hep-lat/0204010].
- [16] C. R. Allton *et al.*, Phys. Rev. D **71**, 054508 (2005) [arXiv:hep-lat/0501030].
- [17] R. V. Gavai and S. Gupta, Phys. Rev. D **78**, 114503 (2008) [arXiv:0806.2233 [hep-lat]].
- [18] S. Basak *et al.* [MILC Collaboration], PoS **LATTICE2008**, 171 (2008) [arXiv:0910.0276 [hep-lat]].
- [19] F. Karsch *et al.*, arXiv:1011.3130 [hep-lat].
- [20] P. de Forcrand and O. Philipsen, Nucl. Phys. B **642**, 290 (2002) [arXiv:hep-lat/0205016].
- [21] M. D’Elia and M. P. Lombardo, Phys. Rev. D **67**, 014505 (2003) [arXiv:hep-lat/0209146].
- [22] L. K. Wu, X. Q. Luo and H. S. Chen, Phys. Rev. D **76**, 034505 (2007) [arXiv:hep-lat/0611035].
- [23] M. D’Elia, F. Di Renzo and M. P. Lombardo, Phys. Rev. D **76**, 114509 (2007) [arXiv:0705.3814 [hep-lat]]. [24]
- [24] S. Conradi and M. D’Elia, Phys. Rev. D **76**, 074501 (2007) [arXiv:0707.1987 [hep-lat]].
- [25] P. de Forcrand and O. Philipsen, JHEP **0811**, 012 (2008) [arXiv:0808.1096 [hep-lat]].
- [26] M. D’Elia and F. Sanfilippo, Phys. Rev. D **80**, 014502 (2009) [arXiv:0904.1400 [hep-lat]].
- [27] J. T. Moscicki, M. Wos, M. Lamanna, P. de Forcrand and O. Philipsen, Comput. Phys. Commun. **181**, 1715 (2010) [arXiv:0911.5682].
- [28] A. Alexandru, M. Faber, I. Horvath and K. F. Liu, Phys. Rev. D **72**, 114513 (2005) [arXiv:hep-lat/0507020].

- [29] S. Kratochvila and P. de Forcrand, PoS **LAT2005**, 167 (2006) [arXiv:hep-lat/0509143].
- [30] S. Ejiri, Phys. Rev. D **78**, 074507 (2008) [arXiv:0804.3227 [hep-lat]].
- [31] M. A. Clark and A. D. Kennedy, Phys. Rev. Lett. **98**, 051601 (2007) [arXiv:hep-lat/0608015].
- [32] Y. Aoki, Z. Fodor, S. D. Katz and K. K. Szabó, JHEP **0601**, 089 (2006) [arXiv:hep-lat/0510084].
- [33] G. I. Egri, Z. Fodor, C. Hoelbling, S. D. Katz, D. Nográdi and K. K. Szabó, Comput. Phys. Commun. **177**, 631 (2007) [arXiv:hep-lat/0611022].
- [34] J. Cleymans and K. Redlich, Phys. Rev. Lett. **81**, 5284 (1998) [arXiv:nucl-th/9808030].